Rapid Communications

Topological acoustics in coupled nanocavity arrays

M. Esmann, F. R. Lamberti, A. Lemaître, and N. D. Lanzillotti-Kimura*
Centre de Nanosciences et de Nanotechnologies, CNRS, Université Paris-Sud, Université Paris-Saclay, C2N, Avenue de la Vauve, 91120 Palaiseau, France

(Received 3 May 2018; published 11 October 2018)

The Su-Schrieffer-Heeger (SSH) model is likely the simplest one-dimensional concept to study nontrivial topological phases and topological excitations. Originally developed to explain the electric conductivity of polyacetylene, it has become a platform for the study of topological effects in electronics, photonics, and ultracold atomic systems. Here, we propose an experimentally feasible implementation of the SSH model based on coupled one-dimensional acoustic nanoresonators working in the gigahertz-terahertz range. In this simulator it is possible to implement different signs of the nearest-neighbor interaction terms, showing full tunability of all parameters in the SSH model. Based on this concept we construct topological transition points generating nanophononic edge and interface states and propose an easy experimental scheme to directly probe their spatial complex amplitude distribution by well-established optical pump-probe techniques.

DOI: 10.1103/PhysRevB.98.161109

I. INTRODUCTION

The polymer *trans*-polyacetylene consists of a carbon chain with alternating C-C single and double bonds. Despite this simple chemical structure, *trans*-polyacetylene triggered numerous fundamental questions when it was discovered that it becomes electrically conducting upon halogen doping [1,2]. The mechanism behind this extraordinary property is conceptually captured by the celebrated Su-Schrieffer-Heeger (SSH) model [3,4]. Essentially, it describes spin-polarized electrons on a one-dimensional lattice with staggered nearest-neighbor hopping in the tight-binding approximation. This allows the formation of topological solitons [5,6].

The particular importance of the SSH model lies in its ability to provide a simple, yet prototypical example of topological phase transitions in one dimension. This has spurred the study of many classical and quantum-mechanical systems beyond polymers, which also allow a description by the SSH or related two-dimensional models. For example, ultracold atomic quantum gases in optical lattices [7] have been used for the direct measurements of Zak phases (the Berry phase in a one-dimensional periodic medium) [8], for the observation of topological edge states [9], and for topological charge pumping [10,11]. In one- and two-dimensional photonic crystals and waveguides [12–14] topological edge states have also been reported [15–19] allowing one-way optical transport [20,21] if time-reversal symmetry is broken. Very recently, the SSH model was implemented in a polaritonic system, supporting lasing edge modes that are robust to disorder [22] and in macroscopic acoustics [23,24]. Acoustic topological insulators made of coupled helical or ring-shaped waveguides [24–28] and other acoustic-quantum analogs [29–31] show the fruitful progress in this field. Reports on studies of topological effects in nanoacoustics, however, remain sparse.

High-frequency acoustic phonons in the gigahertz-terahertz (GHz-THz) range are relevant in the determination of thermal and electronic transport properties and constitute a main source of decoherence in solid-state quantum systems [32,33]. Acoustic phonons, however, also represent a versatile platform for the study of wave dynamics and localized excitations featuring two main advantages with respect to the electronic and optical counterparts: First, their relatively slow speed of propagation results in wavelengths of few nanometers at 100 GHz-THz frequencies. This allows the experimental implementation of very large systems [34], which may be considered infinite for all practical means [35]. Second, 100 GHz-THz frequencies and slow speeds render the resulting acoustic wave function quasistatic when probed optically giving full access to amplitude and phase information [36]. The fundamental building blocks to confine, shape, and guide phonons at the nanoscale are finite-size superlattices employed as distributed Bragg reflectors (DBRs), phononic Fabry-Perot cavities formed by two DBRs enclosing a resonant spacer layer and coupled cavity arrays [37–39]. Although these versatile elements are well-established devices in nanophononics, their application to the study of topological order has remained greatly unexplored [35,40].

Here we propose to implement the SSH model in acoustic nanocavity arrays working in the 300 GHz range with each cavity representing a carbon atom in polyacetylene. We demonstrate that our implementation supports topologically protected edge and interface states. We furthermore show how to optically address the resulting topological acoustic states with clear, easy to detect signatures by well-established pump-probe experiments. We show how it is possible to experimentally detect a sign reversal of the staggered hopping terms, which allows distinguishing fully symmetric and

*Corresponding author: daniel.kimura@c2n.upsaclay.fr

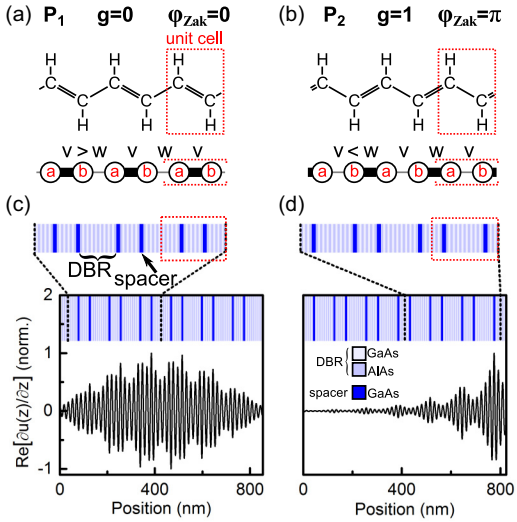

FIG. 1. SSH model in an acoustic nanocavity array. (a),(b) Topological phases P_1 (trivial) and P_2 (nontrivial) of the SSH model with corresponding polyacetylene molecules. (c),(d) Top: P_1 and P_2 implemented in a coupled acoustic nanocavity array. Resonant spacer layers represent atomic sites and distributed Bragg reflectors (DBRs) represent weak and strong hopping links, respectively. Bottom: Strain distributions $\partial u(z)/\partial z$ in cavity arrays of six unit cells. A Bloch-like mode of P_1 (c) and the topological edge mode of P_2 at $f = 300$ GHz (d).

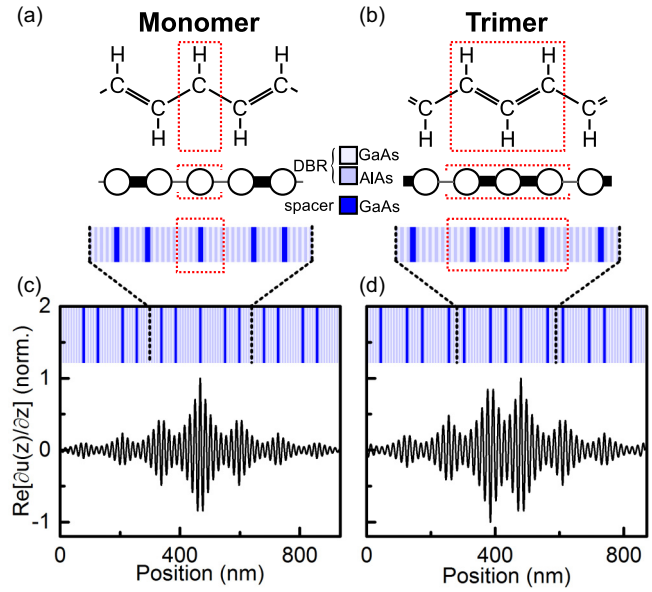

FIG. 2. Mono- and trimerlike SSH interface states in nanophononic cavity array. (a) Monomer defect in polyacetylene and coupled phononic cavities. (b) Trimer defect. (c),(d) Strain distribution of topological monomer (c) and trimer defect states (d) in coupled phononic cavities at $f_0 = 300$ GHz superimposed with the GaAs/AlAs layer structure. DBRs contain 4.5 and 8.5 layer pairs, respectively.

antisymmetric edge states. Our results thus present a critical step forward toward the observation of more complex topology-driven physical effects in nanoacoustics with large potential to optimize interactions with electrons and photons based on topologically engineered structures.

II. RESULTS AND DISCUSSION

The order of the single/double bonds in polyacetylene leads to two energetically degenerate isomers as depicted in Figs. 1(a) and 1(b) (top). Each sp^2-hybridized carbon atom contributes a delocalized π electron subject to the staggered hopping potential across double and single carbon bonds. For a chain of N diatomic unit cells, this situation is captured via the second-quantized single-particle Hamiltonian [3,4,8,9,41]

$$\hat{H} = \sum_{n=1}^{N} v(a_n^\dagger b_n + \text{H.c.}) + w(a_n^\dagger b_{n-1} + \text{H.c.}). \qquad (1)$$

Here, v and w are the intra- and intercell hopping integrals. The operators $a_n^{(\dagger)}$ and $b_n^{(\dagger)}$ annihilate (create) a particle in the nth unit cell on sublattice a or b, respectively.

The two isomers in Figs. 1(a) and 1(b) represent two topologically different phases P_1 and P_2 [41,42]. Essentially, if the intercell hopping dominates ($v < w$), the band structure of an infinite P_2-type lattice is characterized by a nontrivial winding number $g = 1$. Equivalently, a particle moving adiabatically on a closed path in momentum space across the first Brillouin zone acquires a Zak phase [8,41–43] (the analog of a geometric Berry phase [44] for Bloch bands) of $\phi_{\text{Zak}} = \pi$. In contrast, for the topologically trivial phase P_1 intracell hopping dominates ($v > w$) and both g and ϕ_{Zak} are zero. A central prediction of the SSH model is the formation of interface states at topological transition points between the phases P_1 and P_2 [3,4] (see Fig. 2) or between the nontrivial phase P_2 and vacuum [41] when the polymer chain is terminated as shown in Fig. 1(b).

To establish an analog of the Hamiltonian (1) in nanophononics, we start from an individual nanophononic cavity, which is usually constructed from a resonant spacer layer of acoustic thickness $m\lambda/2$ ($m \in \mathbb{N}$, λ acoustic wavelength) between two DBRs. An acoustic DBR is a material with a periodic modulation of its elastic properties and exhibits spectral intervals of high acoustic reflectivity. These stop bands correspond to acoustic band gaps of the equivalent infinite periodic lattice. Choosing alternating layers of acoustic thickness $\lambda/4$, the first acoustic band gap of the DBR is centered at the resonance of the spacer and the structure becomes a Fabry-Perot resonator. Such a cavity constitutes the phononic analog of a one-dimensional atom with two potential barriers enclosing a potential well [34]. Accordingly, its solutions to the acoustic wave equation form a spectrum of resonant modes, which are localized in the spacer layer.

A first extension of this concept is to couple two resonant cavity spacers by placing two DBRs around and one between them. This is the phononic analog of a diatomic molecule [45]. Its resonant modes are symmetric and antisymmetric linear combinations of the individual cavity resonances. For the implementation of the SSH model the key idea is to couple a chain of these phononic dimers. The necessary staggering of the hopping is introduced by DBRs with different numbers of layers (and hence different reflectivities) for the inter- and intracell hopping. The resulting structures are schematically shown in Figs. 1(c) and 1(d) (top). In direct analogy to

the chemical structure of polyacetylene, we identify each Fabry-Perot spacer (dark blue) with a site (a carbon atom) and each DBR with a C-C single or double bond (see Supplemental Material [46]).

As a first example, we simulated the topological phases P_1 and P_2 and demonstrated the emergence of a topological edge state for the nontrivial phase. We designed a structure based on GaAs and AlAs resonant at $f_0 = 300$ GHz, i.e., for an acoustic wavelength of $\lambda = c_{\mathrm{GaAs}}/f_0 = 16$ nm (c_{GaAs} speed of sound in GaAs) in the GaAs spacers. DBRs were simulated with thicknesses of a quarter wavelength per layer such that the first high reflectivity stop band is centered around f_0. In order to establish $v < w$, i.e., the nontrivial phase P_2, we used DBRs of 8.5 layer pairs inside unit cells (16 layers of GaAs and 17 layers of AlAs) and DBRs of 4.5 layer pairs to connect adjacent unit cells. In Figs. 1(c) and 1(d) the result of a corresponding transfer-matrix calculation on a lattice of six diatomic unit cells is shown for both P_2 and P_1. We plotted the mechanical strain distribution in the nanophononic cavity chain at f_0. We indeed observe the formation of a confined edge state at f_0 in P_2 [panel (d)]. In agreement with the SSH model [42] the mode selectively populates sublattice b. That is, the strain exhibits antinodes on each spacer layer of sublattice b and nodes on all sites of sublattice a. Furthermore, subsequent antinodes of the strain alternate in sign. The overall envelope of the edge state decays evanescently into the structure. In contrast, we find no such state for the topologically trivial phase P_1 [panel (c)]. The only resonances in this case are Bloch-like modes, which occupy both sublattices.

Next, we investigate the presence of topological interface states when concatenating the two topological phases P_1 and P_2. In Figs. 2(a) and 2(b) the two possible configurations of an interface are sketched for polyacetylene and for an acoustic nanocavity array. One can either construct a monomerlike defect [panel (a)] represented by one spacer layer connected with two weak hopping links (two wider DBRs) or a trimerlike defect composed of three sites connected by strong hopping links [panel (b)]. Figures 2(c) and 2(d) show the results of corresponding calculations using DBRs of 4.5 and 8.5 layer pairs, respectively. Both the monomer and the trimer state are resonant at f_0 and their strain distributions with exponentially decaying envelopes are localized around the defects in the structures. The strain of the monomer exhibits antinodes of alternating sign on the central defect and on every second other spacer. Antinodes are found on the sites in between. In contrast, the trimerlike state exhibits a node on the central site of the defect and antinodes of opposite sign but equal magnitude on the two outer sites of the defect. In the remainder of the structure, the same behavior as for the monomer is found with antinodes in strain on every other site and nodes in between. These findings are in full agreement with the predictions of the SSH model [42].

The sign of the hopping integrals in the SSH model can be reversed by introducing an additional hopping phase of π as sketched in the insets of Fig. 3. As an example, we discuss this for the topological edge state of P_2. First, consider again the structure composed of sites separated by DBRs of 4.5 and 8.5 layer pairs [Fig. 3(a)]. The phase acquired by a phonon upon propagating between the centers of adjacent lattice sites on sublattice b is $\phi_{AS} = \phi_v + \phi_w + 2\pi$. Here, ϕ_v and ϕ_w represent the propagation phases through the two DBRs and the additional phase of 2π accounts for the propagation through the spacer layers. A DBR with m layers leads to a propagation phase of $\phi = m\pi/2$. In total the phonon therefore picks up a phase of $\phi_{AS} = 15\pi$, which translates into a state with alternating sign of the strain on subsequent sites of sublattice b. We refer to this configuration as an antisymmetric wave function.

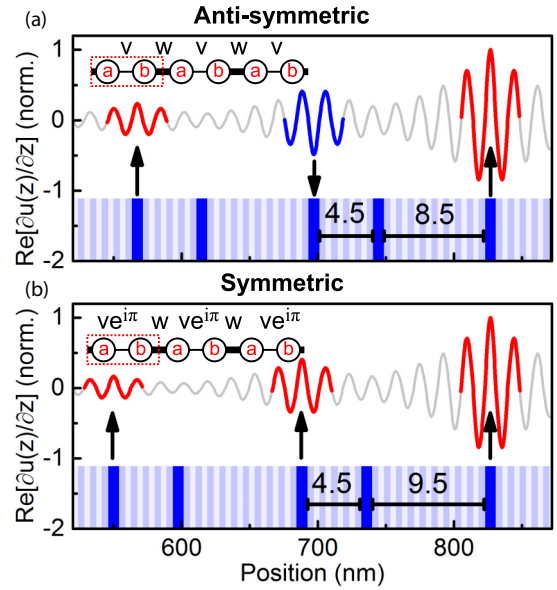

FIG. 3. Symmetric and antisymmetric topological edge states in nanophononic cavity array. (a) Antisymmetric edge state on sublattice b with alternating sign of the strain (red and blue), and layer structure with alternating DBRs of 4.5 and 8.5 layer pairs. (b) Symmetric edge state. By the addition of one layer pair in the thicker DBRs the hopping integral acquires an additional phase of π.

In Fig. 3(b), we repeated the calculation but added one extra pair of layers to each DBR of type v (i.e., 9.5 instead of 8.5). The overall propagation phase between neighboring sites on sublattice b hence changes to $\phi_S = 16\pi$. This changes the symmetry of the state with all nodes of the strain on sublattice b oscillating in phase. We hence term this configuration a symmetric wave function. We note that, in principle, the additional propagation phase can be gauged away in the SSH model by incorporating it into the basis states [9,42]. Thus, all considerations above concerning topological phases and winding numbers still hold. Nevertheless, as we will see shortly, the change in mode symmetry has a significant impact on the experimental signatures of the topological states in optical detection.

In the last part, we discuss the experimental feasibility of detecting the dynamics in a particular acoustic atom of a coupled nanocavity array by optical means. To this end, we simulated pump-probe spectroscopy measurements [47–49].

In this technique, the coherent generation and detection of acoustic phonons in the GHz-THz range are based on ultrashort laser pulses. A first pulse interacts with the sample, generating coherent acoustic phonons [50]. The resulting coherent vibrations induce changes in the optical reflectivity of the sample. A second delayed pulse probes the instantaneous

optical reflectivity of the sample. By systematically changing the delay between the pump and probe pulse the time-resolved reflectivity of the sample and hence the dynamic evolution of the phonons generated by the pump is reconstructed. Coherent longitudinal acoustic phonons can propagate over macroscopic distances, even at room temperature [38,51]. The associated lifetimes are hence long enough as to evidence the dynamics of the topological states studied here.

The phonon generation can be localized in a metallic thin film at the sample surface [52–56], launching a broadband acoustic pulse into the semiconductor sample, whereas the detection takes place inside the semiconductor itself [49,57–60]. By engineering the electronic levels in the superstructure, it is possible to perform a spatially selective detection of strain. In particular, it is possible to probe the strain dynamics in a single cavity spacer (see Supplemental Material [46]).

To simulate the experiment described above, we consider a broadband, Fourier-limited phonon pulse generated outside the topological structure [38]. For the amplitude spectrum $g(\omega)$ of the pulse we choose a Gaussian centered at $f_0 = 300$ GHz with a full width of $2\Delta f = 40$ GHz ($2\Delta\omega = 251$ GHz):

$$g(\omega) \propto \frac{1}{\sqrt{2\pi}\,\Delta\omega} \exp\left(-\frac{(\omega-\omega_0)^2}{2\,\Delta\omega^2}\right). \tag{2}$$

The time-resolved reflectivity $\Delta R(t)$ is modeled by calculating the photoelastic overlap integral [47,61]

$$\Delta R(t) \propto \int_0^L p(z)\frac{\partial u(z,t)}{\partial z} E_p^2(z)dz. \tag{3}$$

Here, L is the length of the phononic structure, $\partial u(z,t)/\partial z$ the strain associated to the propagating phonon pulse, and $E_p(z)$ the electric field of the probe pulse. For $E_p(z)$ we use a standing wave pattern [47], which can, for example, be generated by an optical DBR placed between the acoustic nanocavity array and the substrate. $p(z)$ is the material-dependent photoelastic constant. If the probe pulse covers an electronic transition in the system, $p(z)$ exhibits a resonance [61]. This enables localized detection schemes [48,49]: GaAs layers can be doped with indium, inducing a local redshift of the electronic transition without considerably modifying the elastic behavior of the layer. In this way, a *single* spacer inside a coupled cavity structure becomes a selective detector for coherent acoustic phonons.

Let us analyze two distinct cases of topological cavity arrays. The first array [inset of Fig. 4(a)] supports a symmetric monomer state, i.e., the wave function of the topological interface state presents maxima of equal (positive) sign on neighboring unit cells. The second array [inset of Fig. 4(b)] also supports a monomer interface state, but the wave function maxima on neighboring unit cells are of opposite sign (indicated with blue and red). This staggered symmetry is achieved by adding one layer pair to every other DBR following the concept in Fig. 3. Figures 4(a) and 4(b) (left panels) show simulated time traces when the central (left-of-center) spacer is selectively addressed (indicated by black and green dots) by setting $p(z)$ constant inside and zero outside the spacer. In both cases, we observe an exponentially decaying envelope, reflecting the phonon lifetime of the cavity array. The signal is

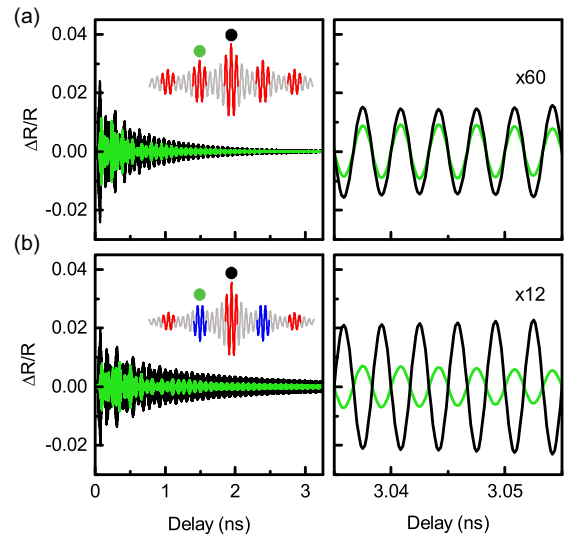

FIG. 4. Simulated transient reflectivity traces of topological states in acoustic nanocavity arrays. (a) Left: Symmetric topological monomer state at 300 GHz (3.5 and 6.5 layer pairs per DBR). Time traces are simulated for photoelastic contributions from the central (black) and left-of-center (green) spacer layer. Right: Zoomed-in time traces showing in-phase modulation of both cavity signatures. (b) Left: Antisymmetric topological monomer state (3.5 and 7.5 layer pairs per DBR). Right: Zoomed-in time traces presenting out-of-phase modulation indicating out-of-phase oscillation of the strain in the central and left-of-center cavity. The quality factors of the topological interface modes are 970 and 2200 for the cases shown in panels (a) and (b).

generated by both confined and propagating phonons of the incident phonon spectrum. The spectral components that do not match any localized eigenstate decay at relatively short times. At sufficiently large times ($\tau > 1$ ns), we hence observe a completely periodic modulation of the transient reflectivity which is dominated by the topological interface state.

By selectively probing spacers in two consecutive unit cells of the symmetric structure [panel (a)] we observe in-phase transient reflectivity traces (see zoomed-in right panel). Conversely, for the antisymmetric wave function [panel (b)], the time traces are in phase opposition. Comparing time traces is hence a direct measure for the symmetry properties of topological acoustic interface states in coupled cavities. By subsequently addressing each acoustic atom separately, the full dynamics of the system becomes accessible.

III. CONCLUSIONS AND OUTLOOK

In this work, we presented an implementation of the SSH model based on coupled acoustic nanocavities. Each nanocavity plays the role of a carbon atom in polyacetylene and the DBRs determine the complex coupling constants between them.

We analyzed cases of typically ten coupled cavities, where by tuning the reflectivity of the mirrors we were able to control the topological winding numbers of the structures. The simplicity of this mapping allowed us to easily study key cases such as the confinement in monomer and trimer states, and symmetric and antisymmetric acoustic states. The proposed

toolbox is compatible with optical probes. By combining bottom-up and top-down technologies it would be possible to extend the presented concepts to higher dimensionalities. For instance, the idea of a three-dimensional nanophononic resonator, representing an acoustic artificial atom, has been recently reported [36,62].

Coherent pump-probe experiments are not only a sensitive tool for the detection of confined acoustic states at topological transition points, but also give valuable insight into their symmetry properties by selectively addressing the strain in individual acoustic atoms. In other words, we presented a simple structure able to mimic the topological physics of polyacetylene and proposed a standard optical experiment to probe the full resulting phonon dynamics. These results represent a first step in the simulation of more complex Hamiltonians. For instance, the implementation of time-reversal symmetry breaking schemes, active phononic materials, exploring anharmonicity effects or tunable and reconfigurable phononic systems in topological arrays of coupled cavities are just some examples among the exciting perspectives of this work.

ACKNOWLEDGMENTS

The authors acknowledge funding through the ERC Starting Grant No. 715939 Nanophennec, and through a public grant overseen by the French National Research Agency (ANR) as part of the "Investissements d'Avenir" program (Labex NanoSaclay, reference: ANR-10-LABX-0035).

[1] C. K. Chiang, C. R. Fincher, Y. W. Park, A. J. Heeger, H. Shirakawa, E. J. Louis, S. C. Gau, and A. G. MacDiarmid, Phys. Rev. Lett. **39**, 1098 (1977).
[2] A. J. Heeger, Angew. Chem., Int. Ed. **40**, 2591 (2001).
[3] W. P. Su, J. R. Schrieffer, and A. J. Heeger, Phys. Rev. Lett. **42**, 1698 (1979).
[4] W. P. Su, J. R. Schrieffer, and A. J. Heeger, Phys. Rev. B **22**, 2099 (1980).
[5] R. Jackiw and C. Rebbi, Phys. Rev. D **13**, 3398 (1976).
[6] A. J. Heeger, S. Kivelson, J. R. Schrieffer, and W.-P. Su, Rev. Mod. Phys. **60**, 781 (1988).
[7] M. Greiner, O. Mandel, T. Esslinger, T. W. Hänsch, and I. Bloch, Nature (London) **415**, 39 (2002).
[8] M. Atala, M. Aidelsburger, J. T. Barreiro, D. Abanin, T. Kitagawa, E. Demler, and I. Bloch, Nat. Phys. **9**, 795 (2013).
[9] E. J. Meier, F. A. An, and B. Gadway, Nat. Commun. **7**, 13986 (2016).
[10] S. Nakajima, T. Tomita, S. Taie, T. Ichinose, H. Ozawa, L. Wang, M. Troyer, and Y. Takahashi, Nat. Phys. **12**, 296 (2016).
[11] M. Lohse, C. Schweizer, O. Zilberberg, M. Aidelsburger, and I. Bloch, Nat. Phys. **12**, 350 (2016).
[12] L. Lu, J. D. Joannopoulos, and M. Soljaĉić, Nat. Photonics **8**, 821 (2014).
[13] A. V. Poshakinskiy, A. N. Poddubny, L. Pilozzi, and E. L. Ivchenko, Phys. Rev. Lett. **112**, 107403 (2014).
[14] M. Xiao, Z. Q. Zhang, and C. T. Chan, Phys. Rev. X **4**, 021017 (2014).
[15] M. Hafezi, S. Mittal, J. Fan, A. Migdall, and J. M. Taylor, Nat. Photonics **7**, 1001 (2013).
[16] N. Malkova, I. Hromada, X. Wang, G. Bryant, and Z. Chen, Opt. Lett. **34**, 1633 (2009).
[17] W. Tan, Y. Sun, H. Chen, and S.-Q. Shen, Sci. Rep. **4**, 3842 (2014).
[18] C. Poli, M. Bellec, U. Kuhl, F. Mortessagne, and H. Schomerus, Nat. Commun. **6**, 6710 (2015).
[19] W. S. Gao, M. Xiao, C. T. Chan, and W. Y. Tam, Opt. Lett. **40**, 5259 (2015).
[20] X. Chen, Z.-C. Gu, Z.-X. Liu, and X.-G. Wen, Science **338**, 1604 (2012).
[21] Y. Lumer, Y. Plotnik, M. C. Rechtsman, and M. Segev, Phys. Rev. Lett. **111**, 263901 (2013).
[22] P. St-Jean, V. Goblot, E. Galopin, A. Lemaître, T. Ozawa, L. L. Gratiet, I. Sagnes, J. Bloch, and A. Amo, Nat. Photonics **11**, 651 (2017).
[23] M. Xiao, G. Ma, Z. Yang, P. Sheng, Z. Q. Zhang, and C. T. Chan, Nat. Phys. **11**, 240 (2015).
[24] C. He, X. Ni, H. Ge, X.-C. Sun, Y.-B. Chen, M.-H. Lu, X.-P. Liu, and Y.-F. Chen, Nat. Phys. **12**, 1124 (2016).
[25] R. Süsstrunk and S. D. Huber, Science **349**, 47 (2015).
[26] Y.-G. Peng, C.-Z. Qin, D.-G. Zhao, Y.-X. Shen, X.-Y. Xu, M. Bao, H. Jia, and X.-F. Zhu, Nat. Commun. **7**, 13368 (2016).
[27] M. A. Bandres, M. C. Rechtsman, and M. Segev, Phys. Rev. X **6**, 011016 (2016).
[28] C. He, Z. Li, X. Ni, X.-C. Sun, S.-Y. Yu, M.-H. Lu, X.-P. Liu, and Y.-F. Chen, Appl. Phys. Lett. **108**, 031904 (2016).
[29] C. Shi, M. Dubois, Y. Chen, L. Cheng, H. Ramezani, Y. Wang, and X. Zhang, Nat. Commun. **7**, 11110 (2016).
[30] R. Fleury, D. Sounas, and A. Alù, Nat. Commun. **6**, 5905 (2015).
[31] X. Zhu, H. Ramezani, C. Shi, J. Zhu, and X. Zhang, Phys. Rev. X **4**, 031042 (2014).
[32] T. Grange, N. Somaschi, C. Antón, L. De Santis, G. Coppola, V. Giesz, A. Lemaître, I. Sagnes, A. Auffèves, and P. Senellart, Phys. Rev. Lett. **118**, 253602 (2017).
[33] L. Besombes, K. Kheng, L. Marsal, and H. Mariette, Phys. Rev. B **63**, 155307 (2001).
[34] N. D. Lanzillotti-Kimura, A. Fainstein, B. Perrin, B. Jusserand, O. Mauguin, L. Largeau, and A. Lemaître, Phys. Rev. Lett. **104**, 197402 (2010).
[35] M. Esmann, F. R. Lamberti, P. Senellart, I. Favero, O. Krebs, L. Lanco, C. Gomez Carbonell, A. Lematre, and N. D. Lanzillotti-Kimura, Phys. Rev. B **97**, 155422 (2018).
[36] S. Anguiano, A. E. Bruchhausen, B. Jusserand, I. Favero, F. R. Lamberti, L. Lanco, I. Sagnes, A. Lematre, N. D. Lanzillotti-Kimura, P. Senellart, and A. Fainstein, Phys. Rev. Lett. **118**, 263901 (2017).
[37] M. Trigo, A. Bruchhausen, A. Fainstein, B. Jusserand, and V. Thierry-Mieg, Phys. Rev. Lett. **89**, 227402 (2002).
[38] A. Huynh, N. D. Lanzillotti-Kimura, B. Jusserand, B. Perrin, A. Fainstein, M. F. Pascual-Winter, E. Peronne, and A. Lemaître, Phys. Rev. Lett. **97**, 115502 (2006).

[39] N. D. Lanzillotti-Kimura, A. Fainstein, A. Lemaitre, B. Jusserand, and B. Perrin, Phys. Rev. B **84**, 115453 (2011).
[40] M. Esmann and N. D. Lanzillotti-Kimura, Appl. Sci. **8**, 527 (2018).
[41] P. Delplace, D. Ullmo, and G. Montambaux, Phys. Rev. B **84**, 195452 (2011).
[42] J. K. Asbóth, L. Oroszlány, and A. Pályi, Lect. Notes Phys. 919 (2016).
[43] J. Zak, Phys. Rev. Lett. **62**, 2747 (1989).
[44] M. V. Berry and F. R. S., Proc. R. Soc. London, Ser. A **392**, 45 (1984).
[45] N. D. Lanzillotti-Kimura, A. Fainstein, C. A. Balseiro, and B. Jusserand, Phys. Rev. B **75**, 024301 (2007).
[46] See Supplemental Material at http://link.aps.org/supplemental/10.1103/PhysRevB.98.161109 for full band-structure calculation of coupled acoustic nanocavities and details on the proposed experimental implementation.
[47] N. D. Lanzillotti-Kimura, A. Fainstein, A. Huynh, B. Perrin, B. Jusserand, A. Miard, and A. Lemaître, Phys. Rev. Lett. **99**, 217405 (2007).
[48] M. F. Pascual Winter, G. Rozas, A. Fainstein, B. Jusserand, B. Perrin, A. Huynh, P. O. Vaccaro, and S. Saravanan, Phys. Rev. Lett. **98**, 265501 (2007).
[49] O. Matsuda, T. Tachizaki, T. Fukui, J. J. Baumberg, and O. B. Wright, Phys. Rev. B **71**, 115330 (2005).
[50] P. Ruello and V. E. Gusev, Ultrasonics **56**, 21 (2015).
[51] R. Legrand, A. Huynh, B. Jusserand, B. Perrin, and A. Lemaître, Phys. Rev. B **93**, 184304 (2016).
[52] N. D. Lanzillotti-Kimura, A. Fainstein, B. Perrin, B. Jusserand, A. Soukiassian, X. X. Xi, and D. G. Schlom, Phys. Rev. Lett. **104**, 187402 (2010).
[53] E. Péronne and B. Perrin, Ultrasonics **44**, e1203 (2006).
[54] C. Thomsen, H. T. Grahn, H. J. Maris, and J. Tauc, Phys. Rev. B **34**, 4129 (1986).
[55] C. Thomsen, J. Strait, Z. Vardeny, H. J. Maris, J. Tauc, and J. J. Hauser, Phys. Rev. Lett. **53**, 989 (1984).
[56] P. M. Walker, J. S. Sharp, A. V. Akimov, and A. J. Kent, Appl. Phys. Lett. **97**, 073106 (2010).
[57] A. Fainstein, N. D. Lanzillotti-Kimura, B. Jusserand, and B. Perrin, Phys. Rev. Lett. **110**, 037403 (2013).
[58] R. Legrand, A. Huynh, B. Perrin, N. D. Lanzillotti-Kimura, and A. Lemaître, Int. J. Thermophys. **34**, 1727 (2013).
[59] C.-K. Sun, J.-C. Liang, and X.-Y. Yu, Phys. Rev. Lett. **84**, 179 (2000).
[60] A. Bartels, T. Dekorsy, H. Kurz, and K. Köhler, Appl. Phys. Lett. **72**, 2844 (1998).
[61] N. D. Lanzillotti-Kimura, A. Fainstein, and B. Jusserand, Ultrasonics **56**, 80 (2015).
[62] F. R. Lamberti, Q. Yao, L. Lanco, D. T. Nguyen, M. Esmann, A. Fainstein, P. Sesin, S. Anguiano, V. Villafañe, A. Bruchhausen, P. Senellart, I. Favero, and N. D. Lanzillotti-Kimura, Optics Express **25**, 24437 (2017).